Peptide antisense nanoparticles

Pinal C. Patel, David A. Giljohann, Dwight S. Seferos, and Chad A. Mirkin[1]

Department of Chemistry and International Institute for Nanotechnology, Northwestern University, Evanston, IL 60208-3113

Edited by Robert H. Austin, Princeton University, Princeton, NJ, and approved May 28, 2008 (received for review February 18, 2008)

We have designed a heterofunctionalized nanoparticle conjugate consisting of a 13-nm gold nanoparticle (Au NP) containing both antisense oligonucleotides and synthetic peptides. The synthesis of this conjugate is accomplished by mixing thiolated oligonucleotides and cysteine-terminated peptides with gold nanoparticles in the presence of salt, which screens interactions between biomolecules, yielding a densely functionalized nanomaterial. By controlling the stoichiometry of the components in solution, we can control the surface loading of each biomolecule. The conjugates are prepared easily and show perinuclear localization and an enhanced gene regulation activity when tested in a cellular model. This heterofunctionalized structure represents a new strategy for preparing nanomaterials with potential therapeutic applications.

gene regulation | gold nanoparticles | heterofunctional

Nucleic acids, such as antisense oligonucleotides and small interfering RNAs, are important research tools for gene function analysis and are widely considered to be potential therapeutics (1, 2). The advantage of nucleic acid–based methods for genetic regulation is their selectivity toward a complementary target conferred by Watson–Crick base pairing. However, the delivery of nucleic acids into mammalian cells remains a major challenge, because cells are naturally resistant to the uptake of genetic material and contain a variety of mechanisms that degrade nucleic acids (3). In recent years, we have discovered that oligonucleotide nanoparticle conjugates act as a single-entity agent, capable of transfecting cells and regulating intracellular gene expression (4). These antisense particles readily enter cells without transfection agents because of their oligonucleotide functionalization (5), are highly resistant toward degradation by enzymes (4), have binding constants that are as much as 2 orders of magnitude greater than oligonucleotides that are free in solution (6), and can be modified with potent designer materials such as locked nucleic acids (7). Thus, these antisense particles overcome many of the challenges associated with the use of oligonucleotides as genetic regulators.

During the past decade, oligonucleotide nanoparticle conjugates (DNA-Au NPs) have been developed for numerous molecular diagnostics assays (8) and self-assembly strategies (9). For example, DNA-Au NPs have been used for the detection of nucleic acids (10–15), small molecules (16, 17), metal ions (18), ultrasensitive detection of proteins (19–24), and intracellular mRNA (25). In addition, these materials have been used in the synthesis of crystalline materials with predefined structures (26, 27).

These advances have been enabled by new synthetic methods for the preparation of Au NP–biomolecule conjugates. To date, these efforts have primarily focused on 2 classes of materials: homofunctionalized nanoparticles that incorporate 1 biomolecule functionality, such as DNA (9, 12), peptides (28, 29), or antibodies (30), and heterofunctionalized nanoparticles including conjugates that combine oligonucleotides and antibodies (22), protein-stabilized DNA-peptide conjugates (31), alkyl chains and plasmid DNA (32), or polyethylene glycol and peptides (33).

On a molecular level, significant research has been devoted toward creating materials incorporating peptides and oligonucleotides because these types of chimeric structures have been shown to increase the knockdown of target proteins (34–43). However, molecular methods of preparing these materials are relatively inefficient, limit sequence diversity because of incompatible chemistries, require orthogonal protecting groups on nucleosides and amino acids (44), and can generate undesired side products (45). Thus, the synthesis and purification of heterofunctional molecules is a challenge.

Here, we demonstrate that an Au NP can be used as a scaffold to combine cysteine-terminated peptides and thiol-terminated oligonucleotides in a straightforward manner. The resulting heterofunctionalized conjugate contains a dense monolayer of both antisense oligonucleotides to glyceraldehyde phosphate dehydrogenase (GAPDH) and peptides. GAPDH was used as the target because it is produced at high levels in most cell types and thus is representative of a general class of high-abundance proteins. The peptides used in this study were selected because of their demonstrated ability to increase cellular uptake and/or alter intracellular localization (34, 35). In contrast to molecular materials, these conjugates can be purified and isolated simply by centrifugation and further allow the control of control oligonucleotide and peptide stoichiometries. In addition, these conjugates exhibit enhanced binding to complementary oligonucleotides, high cellular uptake, and the ability to regulate gene expression. When evaluated in a cell model, these heterofunctionalized conjugates demonstrate up to 75% gene knockdown.

Results and Discussion

Heterofunctionalized nanoparticle conjugates containing both peptides and oligonucleotides were prepared by adding oligonucleotides terminated with a 3′-propylthiol functionality and peptides terminated with an N-terminal cysteine residue (stoichiometric ratios ranged from 1:2 to 16:1) to a buffered solution containing Au NPs, 0.1% Tween-20, and 0.2M NaCl (Fig. 1*A*). The addition of salt before adding the peptides and oligonucleotides is critical, because the salt screens the electrostatic attraction between the oligonucleotides and peptides and leads to stable conjugates. Without the pre-addition of salt, the nanoparticles became unstable during the preparation procedure, as indicated by the red-shifting of the gold plasmon peak [supporting information (SI) Table S1]. To complete the functionalization process, the mixture was aged further in solutions of increasing salt concentrations to achieve a 0.3 M final NaCl concentration. Once functionalization was completed, the resulting conjugates were separated from excess unbound ligands

This paper results from the Arthur M. Sackler Colloquium of the National Academy of Sciences, ''Nanomaterials in Biology and Medicine: Promises and Perils,'' held April 10–11, 2007, at the National Academy of Sciences in Washington, DC. The complete program and audio files of most presentations are available on the NAS web site at www.nasonline.org/nanoprobes.

Author contributions: P.C.P., D.A.G., D.S.S., and C.A.M. designed research; P.C.P. performed research; P.C.P., D.A.G., D.S.S., and C.A.M. analyzed data; and P.C.P., D.A.G., D.S.S., and C.A.M. wrote the paper.

The authors declare no conflict of interest.

This article is a PNAS Direct Submission.

[1]To whom correspondence should be addressed. E-mail: chadnano@northwestern.edu.

This article contains supporting information online at www.pnas.org/cgi/content/full/0801609105/DCSupplemental.

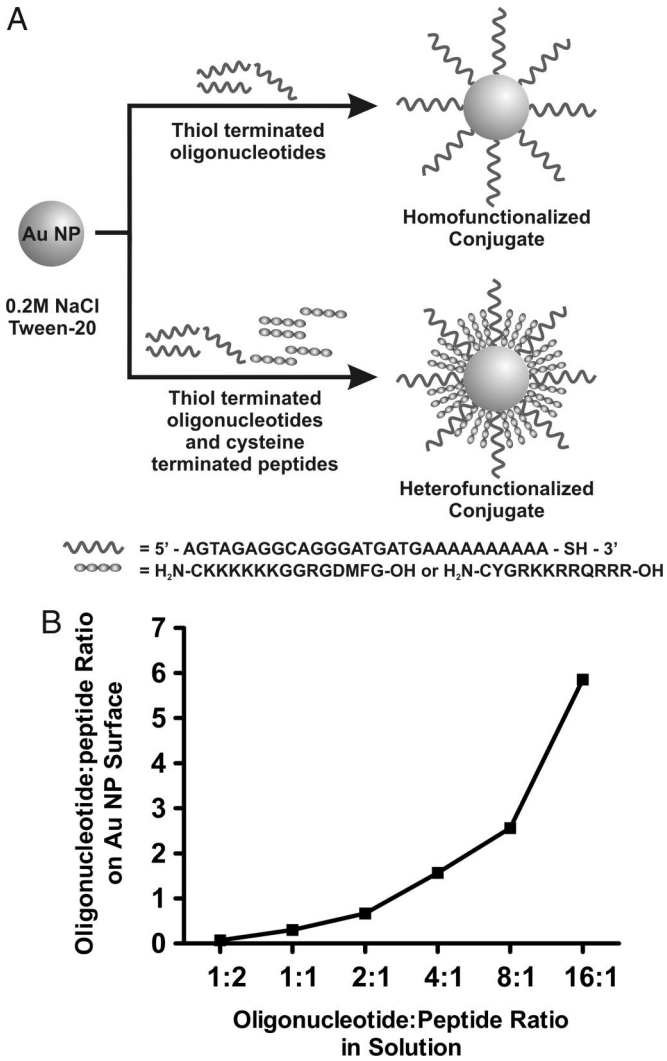

Fig. 1. Preparation of peptide and oligonucleotide functionalized gold nanoparticles. (*A*) Oligonucleotides were modified with a 3′ thiol group, and peptides were synthesized with an N-terminal cysteine to facilitate attachment to the gold nanoparticle surface. The key to creating the peptide ASNPs is the addition of salt before the addition of biomolecules to screen the charges. (*B*) Oligonucleotide and peptide loading as a function of solution stoichiometry on 13-nm gold nanoparticles determined by fluorescent labeling.

by centrifugation and were characterized for surface charge, polarity, and hydrodynamic radii (Table S2).

To characterize the degree of nanoparticle surface functionalization, the numbers of attached oligonucleotides and peptides per Au NP were determined by fluorescence methods (see *Materials and Methods*) (46). The results of these studies demonstrate that, although there is not a 1:1 correlation, the solution stoichiometry (oligonucleotides and peptides) can be used to control the surface composition of the nanoparticle (Fig. 1*B*). For example, at a 1:2 oligonucleotide to peptide ratio in solution, a 1:5 ratio is obtained on the nanoparticle surface. If the oligonucleotide concentration in solution is held constant (1.7 nmol/ml), an increase in peptide concentration results in a nanoparticle conjugate with an increased peptide loading and a decreased oligonucleotide loading. For example, at a solution molar ratio of 1:1 (oligonucleotides to peptide), the surface composition is 68 ± 5 (oligonucleotides) and 225 ± 31 (peptides) per nanoparticle. At a solution molar ratio of 2:1 (oligonucleotide to peptide), the average number of oligonucleotides and peptides is 83 ± 7 and 124 ± 7, respectively. These studies allow us to determine what solution stoichiometry is needed to provide a given nanoparticle composition. In all cases a dense loading of oligonucleotide is achieved during co-functionalizing with peptides.

Fluorescence-based characterization reveals that this synthetic method yields nanoparticle conjugates functionalized with both oligonucleotides and peptide sequences. Because Watson–Crick recognition is a critical step in antisense gene regulation, we next investigated the ability of these peptide antisense particles to bind complementary oligonucleotide targets. For these studies we used particles prepared from a solution with a 1:1 molar ratio of peptides and oligonucleotides because this ratio yields a conjugate that is functionalized with ≈50% of the observed maximum for each biomolecule (Fig. S1). An oligonucleotide sequence complementary to this candidate particle and containing a terminal fluorophore (FAM) was allowed to hybridize to the nanoparticle conjugates as described previously (6). In the hybridized state, the fluorescence of FAM is quenched significantly because of its proximity to the Au NP surface. The solution was heated slowly while the fluorescence signal was measured to monitor the transition from the hybridized to unhybridized state. These studies demonstrate that nanoparticles co-functionalized with oligonucleotides and with either nuclear localization signal (NLS) (T_m = 73 ± 0.4°C) or Tat peptides (T_m = 71 ± 0.2°C) display nearly identical melting temperatures, and a noncomplementary oligonucleotide sequence did not display a melting transition (see Fig. S2). Importantly, these high melting temperatures are consistent with the melting temperature of ASNPs without peptides (T_m = 72 ± 0.7°C). It should be noted that the binding affinities of ASNPs are as much as 2 orders of magnitude greater than the same oligonucleotides free in solution (i.e., not attached to an Au NP) (6). These melting experiments indicate that the addition of peptides has little observable effect on the affinity of the ASNPs for their complement. It has been shown previously that conjugation of oligonucleotides to basic peptides increases their affinity for their complement as determined by an increase in T_m of 1° to 2.5°C (47). However, if there is a similar effect in this system, it is relatively small in comparison with the enhanced affinity for complementary target that results from a dense loading of oligonucleotides on Au NPs (6, 48).

Having established the high surface-loading and high binding affinities of the peptide ASNP conjugates, we next investigated the intracellular activity of these novel conjugates in HeLa cells. HeLa cells were treated with peptide antisense particles for 48 h, and the amount of GAPDH was quantified using Western blotting. Analogous nanoparticles with a sequence noncomplementary to GAPDH were used as controls. These studies demonstrate that peptide antisense particles are more effective at down-regulating GAPDH than antisense particles without peptides. (A representative Western blot is shown Fig. 2*A*). For example, antisense particles containing Tat or NLS peptides decreased GAPDH expression by 78% ± 13% and 75% ± 10%, respectively, at 40-nM nanoparticle concentration. An identical concentration of antisense nanoparticles resulted in a 53% ± 7% decrease in GAPDH expression. Therefore, in this example, the addition of peptides to antisense nanoparticles increases efficacy by ≈50%. This antisense activity is comparable to using molecular peptide-oligonucleotide conjugates at more than 5 times the concentration of the agent described here (49, 50). All control nanoparticles with noncomplementary oligonucleotide sequences, including those containing Tat and NLS peptides, had no visible effect on GAPDH levels. In addition, at high concentrations of peptide antisense nanoparticles, a noticeable decrease in cell viability was observed (Table S3). Although cell counts were normalized for Western blotting measurements, we observed a decrease in total cell number for cells treated with

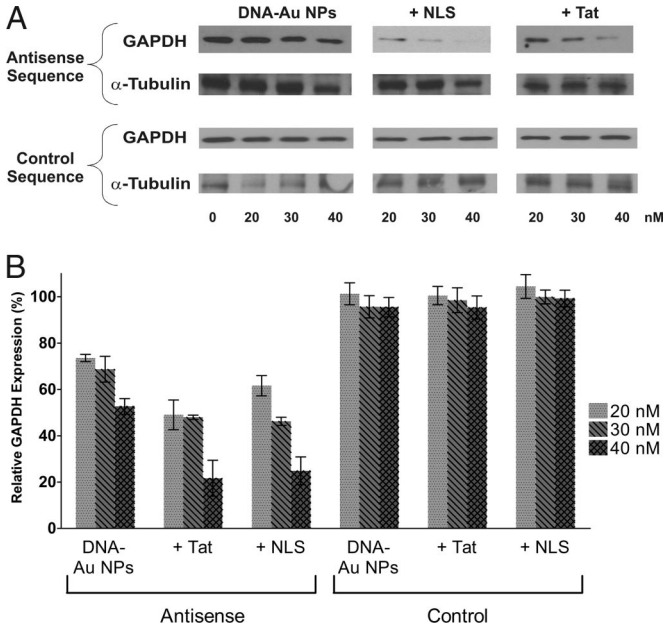

Fig. 2. Activity of peptide antisense nanoparticles. (*A*) Representative Western blots showing the expression of GAPDH in HeLa cells treated with various concentrations and compositions of nanoparticle conjugates. GAPDH expression is reduced in a dose- and sequence-dependent manner. α-Tubulin is shown as the loading control. (*B*) Relative decrease in GAPDH expression in HeLa cells. α-Tubulin was used as a loading control and for subsequent normalization of GAPDH knockdown. The error bars represent the standard deviation from at least 3 Western blots.

anti-GAPDH particles (data not shown), consistent with previous reports showing that down-regulation of GAPDH leads to slower cell growth (51). However, the decreased cell count and viability were observed only in the case of nanoparticles co-functionalized with both the anti-GAPDH oligonucleotides and peptides. No decrease in viability was observed for either type of conjugate containing noncomplementary oligonucleotides.

We investigated whether increased uptake or altered cellular location was the cause of the increased knockdown activity observed for peptide antisense nanoparticles. Mass spectrometry experiments were conducted to quantify the number of internalized particles based on intracellular gold content (5), because one would expect that a higher number of antisense agents per cell would lead to a greater knockdown. The results of these studies show a similar number of nanoparticles per cell for all conjugates (Fig. S3); thus higher uptake of the peptide antisense particles does not seem to be the cause of the observed enhanced knockdown.

Fluorescence imaging experiments were conducted to examine the intracellular localization pattern of the particles because translocation into the nucleus has been shown to increase efficacy of antisense agents (39, 50). For these experiments, nanoparticles were functionalized with fluorescently labeled oligonucleotides. Because the peptides (Fig. S4) and the oligonucleotides have been shown to remain attached to the nanoparticle surface (4), these experiments allow us to determine the intracellular localization of nanoparticles. The results of these experiments are intriguing, because they suggest no gross differences in peptide antisense particle localization as compared with antisense particles. However, closer inspection reproducibly revealed more fluorescence associated with the regions of the cell directly outside the nucleus in the case of peptide antisense nanoparticles (Fig. 3). Because size is a main determinant of the ability of objects to enter the nucleus (52), we changed the core

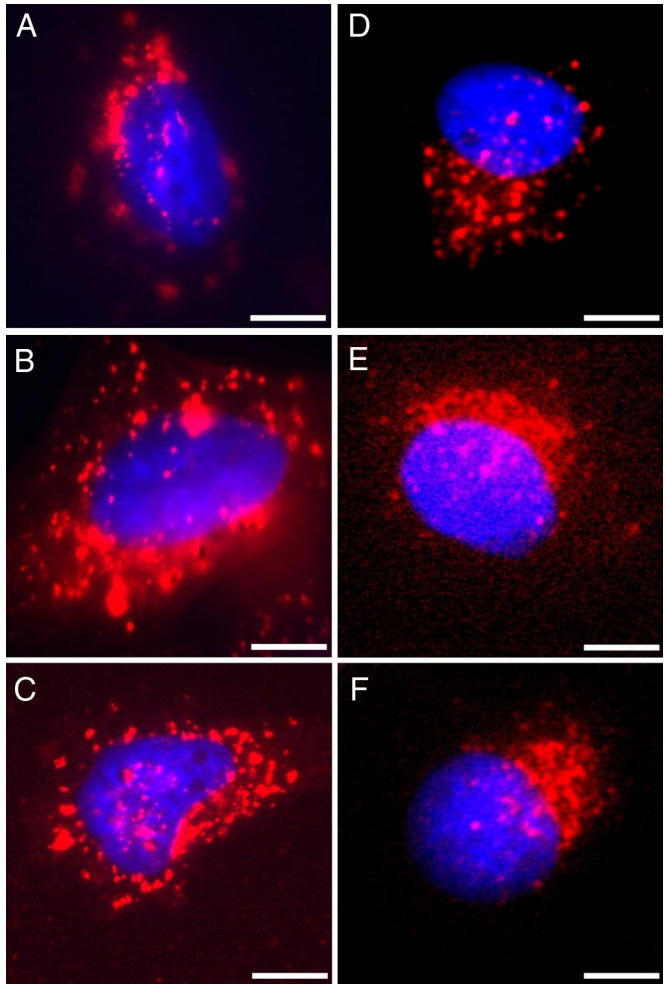

Fig. 3. Confocal fluorescence microscopy images of HeLa cells treated with 13-nm (*A–C*) or 5-nm (*D–F*) antisense particles functionalized with Cy5-terminated oligonucleotides (red) (*A* and *D*), Tat peptides and Cy5-terminated oligonucleotides (*B* and *E*), or NLS peptides and Cy5-terminated oligonucleotides (*C* and *F*). Nucleus (blue) is stained with Hoechst 33342. Scale bar is 10 μm in each image.

size of the peptide antisense particles from 13 nm to 5 nm, expecting that these smaller conjugates would show a more prominent change in cellular localization. However, the results of these experiments show a localization pattern (Fig. 3) similar to that observed for 13-nm peptide antisense particles. Although no definitive intranuclear localization can be seen with either size conjugate, the perinuclear localization pattern that we have observed with peptide antisense particles correlates with the increased knockdown.

Conclusions

We have described the synthesis, characterization, and intracellular testing of peptide antisense particles, a heterofunctionalized Au NP–biomolecule conjugate containing a dense monolayer of thiolated oligonucleotides and cysteine-terminated peptides. We have determined that the addition of salt is necessary for the co-functionalization process to screen electrostatic interactions oligonucleotides and peptides and to prevent irreversible aggregation of the nanoparticles. Following this procedure, the ratio of each component that is immobilized on the Au NP surface can be controlled by varying the stoichiometry of the molecules in solution. The resultant materials have a high loading of both peptides and oligonucleotides, exhibit high

affinity for complementary targets as determined by melting point studies, can be purified easily by centrifugation, and demonstrate effective gene regulation (>75% knockdown of GAPDH). The design considerations, synthetic techniques, and subsequent characterization of the materials presented in this work pave the way toward creating new generations of hetero-functionalized nanomaterials for a variety of diagnostic and therapeutic applications.

Materials and Methods

Materials. Citrate-stabilized Au NP (13 ± 1 nm diameter) were prepared as described previously (53). Nanoparticles 5 nm in diameter were purchased from Ted Pella. Oligonucleotides were synthesized on an Expedite 8909 Nucleotide Synthesis System (ABI) using standard solid-phase phosphoramidite synthesis techniques. All bases and reagents, including Cy5 dye (1-[3-(4-monomethoxytrityloxy)propyl]-1′-[3-[(2-cyanoethyl)-(N,N-diisopropyl phosphoramidityl]propyl]-3,3,3′,3′-tetramethylindodicarbocyanine chloride), 3′ C_3H_6-thiol CPG (1-O-Dimethoxytrityl-propyl-disulfide,1′-succinyl-lcaa-CPG), 3′ (6-FAM) CPG (1-Dimethoxytrityloxy-3-[O-(N-carboxyl-(di-O-pivaloyl-fluorescein)-3-aminopropyl)]-propyl-2-O-succinoyl-long chain alkylamino-CPG), and sulfurizing reagent (3H-1,2-Benzodithiole-3-one-1,1-dioxide), were purchased from Glen Research. Sulfurizing reagent was used to generate phosphorothioate linkages between the 2 terminal 3′ adenines and the 2 terminal 5′ bases (indicated with an asterisk below). The oligonucleotides were purified using reverse-phase high-performance liquid chromatography (RP-HPLC) using a Varian Microsorb C18 column (10 μm, 300 × 10 mm) with 0.03 M triethylammonium acetate (TEAA), pH 7, and a 1%/min gradient of 95% CH_3CN/5% 0.03 M TEAA at a flow rate of 3 ml/min while monitoring the UV signal of DNA at 254 nm. After purification, the oligonucleotides were lyophilized and stored at − 78°C until use. Before nanoparticle conjugation, the 3′ disulfide functionality was reduced with DTT ((Pierce Biotechnologies) following published procedures (54). The cleaved oligonucleotides were purified using a Sephadex G25 column (Amersham Pharmacia Biotech) and were resuspended in NANOpure water. The sequences used in the melting studies were 5′G*A*GCTCCAC GCTGCCGTCAA AAAAAAA*A* -propylthiol-3′ and 5′GACG-GCAGCGTGGAGC TC–6-FAM-3′. The sequences used in the cell studies were control: 5′A*T*CCTTATC AATATTAAAAAAAAAA*A*-propylthiol-3′ and anti-GAPDH: 5′A*G*TAGAGGCAGG GATGATGAAAAAAAAA*A*-propylthiol-3′.

Oligonucleotide- and Peptide-Oligonucleotide–Functionalized Nanoparticle Preparation. Oligonucleotide-functionalized Au NPs were prepared as described previously (12). For peptide-oligonucleotide particles, peptides including HIV Tat protein signal (Tat), (H_2N-CYGRKKRRQRR R-OH), NLS (H_2N-CKKKKKKGGRGDM FG-OH), and fluorescein-labeled NLS (H_2N-C[Flc]KKKKKKGGRGDMFG-OH) were purchased from Sigma Genosys. The peptide ASNPs were prepared with important modifications to published protocols (54). Tween-20 (Sigma) was added to a citrate-stabilized Au NP solution (9 nM) to achieve a Tween-20 concentration of 0.1%. After 10 min, the solution was brought to 0.2M NaCl and 0.01M phosphate buffer, pH 7.4, and was stirred for 5 minutes. Thiolated oligonucleotides and cysteine-terminated peptides were added to the solution of nanoparticles in different stoichiometries (e.g., 1.7 nmol of each per 1 ml Au NPs in a 1:1 ratio). The final mixture was brought to 0.3M NaCl over 24 h and shaken for an additional 24 h to complete the functionalization process. The particles were centrifuged (16,000 × *g*), resuspended twice with 0.1M Na_2CO_3 and twice with 2× PBS (0.0067M phosphate buffer pH 7.4, 0.3M NaCl), and finally resuspended in 2× PBS.

Oligonucleotide and Peptide Characterization. Au NPs functionalized with oligonucleotides and fluorescein-NLS peptides or oligonucleotides and NLS peptides were prepared as described in the previous sections. The concentrations of the functionalized nanoparticles were determined using UV-visible spectroscopy with $\varepsilon = 2.7 \times 10^8$ liters/(mol·cm). Nanoparticles were dissolved by adding a stock solution of potassium cyanide (KCN; Sigma) to the particles until the final KCN concentration was 0.0025 M. The concentration of released oligonucleotides was determined using a Quant-iT OliGreen ssDNA Assay Kit (Invitrogen). The fluorescence associated with the released DNA was measured (ex: 486 nm, em: 530 nM) and compared with the fluorescence of a standard curve generated from the same oligonucleotide sequence using the same assay protocol. The concentration of fluorescein-labeled NLS peptide was determined by dissolving the particles with KCN (as described in an earlier section), measuring the fluorescence (ex: 486 nm, em: 530 nm), and comparing it with the fluorescence of a standard curve generated from a stock solution of the same peptide. All fluorescence measurements were made on a FluoDia T70 fluorescent plate reader (Photon Technologies International) in Costar-black, clear, flat-bottomed 96-well plates (Corning). Nanoparticles functionalized with oligonucleotides alone or with oligonucleotides and peptides (1:1 solution ratio) were diluted to 1-nM concentration in PBS buffer. Dynamic light-scattering measurements were performed using a polystyrene cuvette at 25°C. Zeta potential measurements were performed in a standard folded capillary cell (Malvern Instruments). Dynamic light-scattering and zeta potential measurements were performed on Zetasizer Nano (Malvern Instruments). For peptide desorption measurements nanoparticles were incubated at 37°C for 24 and 48 h in 2× PBS (pH 7.4), 0.1 M phosphate-citrate buffer (pH 5.0), and HeLa cell culture medium (EMEM with 10% FBS). Following the incubation, the nanoparticles were centrifuged as described previously, and fluorescence measurements were taken from the supernatant and the pellet and were compared with a control sample from the 0-h time point.

Melting Point Determination. Au NPs functionalized with peptides and oligonucleotides (1:1 molar ratio) or oligonucleotides alone were suspended in 2× PBS at 5 nM concentration in the presence of equimolar concentration of 3′ FAM-labeled complementary or noncomplementary oligonucleotides. The mixture was heated to 65°C for 30 min and cooled to room temperature overnight (at least 12 h). Melting experiments were carried out on a Jobin Yvon Fluorolog FL3–22 by measuring the fluorescence (ex: 492; em: 520) while increasing the sample temperature in 1° increments with a 5-minute equilibration time at each temperature. At least 3 independent experiments were performed for each sample, and results were averaged.

Cell Culture and Nanoparticle Transfections. HeLa cells (ATCC) were maintained in 5% CO_2 at 37°C in DMEM supplemented with 10% heat-inactivated FBS (ATCC) and penicillin/streptomycin (penicillin, 100 units/ml; streptomycin, 100 μg/ml). Cells were seeded at a density of 15,000 cells per well in a 96-well plate and grown for 24 h. After 24 h, the cells were washed with 1X PBS (HyClone), and fresh medium was added. Functionalized particles were filtered (20-μm acetate filter, GE) and were added to the cells at 20-, 30-, and 40-nM concentrations. After 48 h, the cells were washed with 1X PBS, were detached from the flasks using the enzyme trypsin-EDTA (ATCC), and were resuspended in DMEM. The cell viability and total cell number were determined using an Easycyte Mini cell counter (Guava Technologies). Cells were centrifuged at 5000 rpm for 10 min to remove excess medium and were lysed in KDalert™ Lysis Buffer (Ambion). The concentration of each sample (cells per ml) was normalized before Western blotting experiments.

Western Blotting. Lysates were electrophoresed through a 4%–12% gradient SDS polyacrylamide gel (SDS/PAGE; Cambrex) and transferred onto a 0.45-μm nitrocellulose membrane (Bio-Rad). Membranes were blocked for 60 min at room temperature with Superblock in Tris-buffered saline (Pierce) and incubated with a mouse anti-human antibody for α-tubulin (Santa Cruz) for 60 min. The membrane then was incubated with goat anti-mouse secondary antibody (Santa Cruz). The membrane was visualized with luminescent reagents (Pierce) and recorded on film (Kodak Biomax). Following thorough washing with Tris-buffered saline (Pierce), the membrane was stripped with Restore Plus Western Blot stripping buffer (Pierce). GAPDH was visualized using mouse anti-human antibody to GAPDH (Chemicon) and goat anti-mouse secondary antibody (Santa Cruz,) following an analogous procedure, as stated previously. Photographs of blots were scanned and analyzed using Scion Image v4.0 (Scion). Knockdown was determined after normalizing to the intensity of the α-tubulin band.

Cell Imaging. HeLa cells were grown on glass coverslips and treated with Au NPs as described previously. Cy5-terminated oligonucleotides were used for imaging experiments. Nanoparticles functionalized with oligonucleotides and peptides, and oligonucleotides alone then were added to the wells (12 nM). After 6 h, cells were washed with 1X PBS, treated with 1 μM Hoechst 33342 (Sigma), fixed in 3% formalin solution, and mounted on glass slides for imaging. All imaging was performed using an Axiovert 200 inverted microscope equipped with a HBO 100W mercury vapor short arc lamp and a 63× oil-immersion objective (Carl Zeiss, Inc.). In all experiments, the pinhole and gain settings of the individual collection channel were adjusted using untreated control cells. These settings were held constant throughout the experiment.

Inductively Coupled Plasma Mass Spectrometry. HeLa cells were grown and treated with particles as described previously. Forty-eight hours after particle addition, the cells were washed twice with 1x PBS, counted, measured for viability, and prepared for inductively coupled plasma mass spectrometry (ICP-MS; Thermo-Fisher) by dissolving samples in an equal volume of 3% HNO_3.

Experimental ICP values were compared with values obtained from a standard curve generated using gold ICP-MS standard (Sigma) and the same matrix (5).

ACKNOWLEDGMENTS. C.A.M. received a grant from the Defense Advanced Research Agency and a Center of Cancer Nanotechnology Excellence grant for support of this research. C.A.M. also received a National Institutes of Health Director's Pioneer Award. D.S.S. received a postdoctoral fellowship supported by the American Cancer Society and the LUNGevity Foundation. P.C.P. is supported by a Malkin Scholarship and a predoctoral Ryan Fellowship.

1. Fire A, *et al.* (1998) Potent and specific genetic interference by double-stranded RNA in *Caenorhabditis elegans*. *Nature* 391:806–811.
2. Wagner RW (1994) Gene inhibition using antisense oligodeoxynucleotides. *Nature* 372:333–335.
3. Lebedeva I, Stein CA (2001) Antisense oligonucleotides: Promise and reality. *Annu Rev Pharmacol Toxicol* 41:403–419.
4. Rosi NL, *et al.* (2006) Oligonucleotide-modified gold nanoparticles for intracellular gene regulation. *Science* 312:1027–1030.
5. Giljohann DA, *et al.* (2007) Oligonucleotide loading determines cellular uptake of DNA-modified gold nanoparticles. *Nano Lett* 7:3818–3821.
6. Lytton-Jean AK, Mirkin CA (2005) A thermodynamic investigation into the binding properties of DNA functionalized gold nanoparticle probes and molecular fluorophore probes. *J Am Chem Soc* 127:12754–12755.
7. Seferos DS, Giljohann DA, Rosi NL, Mirkin CA (2007) Locked nucleic acid-nanoparticle conjugates. *Chembiochem* 8:1230–1232.
8. Rosi NL, Mirkin CA (2005) Nanostructures in biodiagnostics. *Chem Rev* 105:1547–1562.
9. Alivisatos AP, *et al.* (1996) Organization of 'nanocrystal molecules' using DNA. *Nature* 382:609–611.
10. He L, *et al.* (2000) Colloidal Au-enhanced surface plasmon resonance for ultrasensitive detection of DNA hybridization. *J Am Chem Soc* 122:9071–9077.
11. Maxwell DJ, Taylor JR, Nie S (2002) Self-assembled nanoparticle probes for recognition and detection of biomolecules. *J Am Chem Soc* 124:9606–9612.
12. Mirkin CA, Letsinger RL, Mucic RC, Storhoff JJ (1996) A DNA-based method for rationally assembling nanoparticles into macroscopic materials. *Nature* 382:607–609.
13. Nie B, Shortreed MR, Smith LM (2006) Quantitative detection of individual cleaved DNA molecules on surfaces using gold nanoparticles and scanning electron microscope imaging. *Anal Chem* 78:1528–1534.
14. Qin WJ, Yung LY (2007) Nanoparticle-based detection and quantification of DNA with single nucleotide polymorphism (SNP) discrimination selectivity. *Nucleic Acids Res* 35:e111.
15. Stoeva SI, Lee JS, Thaxton CS, Mirkin CA (2006) Multiplexed DNA detection with biobarcoded nanoparticle probes. *Angew Chem Int Ed Engl* 45:3303–3306.
16. Han MS, Lytton-Jean AK, Oh BK, Heo J, Mirkin CA (2006) Colorimetric screening of DNA-binding molecules with gold nanoparticle probes. *Angew Chem Int Ed Engl* 45:1807–1810.
17. Liu J, Lu Y (2005) Fast colorimetric sensing of adenosine and cocaine based on a general sensor design involving aptamers and nanoparticles. *Angew Chem Int Ed Engl* 45:90–94.
18. Lee JS, Han MS, Mirkin CA (2007) Colorimetric detection of mercuric ion (Hg2+) in aqueous media using DNA-functionalized gold nanoparticles. *Angew Chem Int Ed Engl* 46:4093–4096.
19. Georganopoulou DG, *et al.* (2005) Nanoparticle-based detection in cerebral spinal fluid of a soluble pathogenic biomarker for Alzheimer's disease. *Proc Natl Acad Sci USA* 102:2273–2276.
20. Hazarika P, Ceyhan B, Niemeyer CM (2005) Sensitive detection of proteins using difunctional DNA-gold nanoparticles. *Small* 1:844–848.
21. Huang CC, Huang YF, Cao Z, Tan W, Chang HT (2005) Aptamer-modified gold nanoparticles for colorimetric determination of platelet-derived growth factors and their receptors. *Anal Chem* 77:5735–5741.
22. Nam J, Jang K, Groves JT (2007) Detection of proteins using a colorimetric bio-barcode assay. *Nat Protoc* 2:1438–1444.
23. Nam JM, Thaxton CS, Mirkin CA (2003) Nanoparticle-based bio-bar codes for the ultrasensitive detection of proteins. *Science* 301:1884–1886.
24. Xu X, Han MS, Mirkin CA (2007) A gold-nanoparticle-based real-time colorimetric screening method for endonuclease activity and inhibition. *Angew Chem Int Ed Engl* 46:3468–3470.
25. Seferos DS, Giljohann DA, Hill HD, Prigodich AE, Mirkin CA (2007) Nano-flares: Probes for transfection and mRNA detection in living cells. *J Am Chem Soc* 129:15477–15479.
26. Park SY, *et al.* (2008) DNA-programmable nanoparticle crystallization. *Nature* 451:553–556.
27. Nykypanchuk D, Maye MM, van der Lelie D, Gang O (2008) DNA-guided crystallization of colloidal nanoparticles. *Nature* 451:549–552.
28. Porta F, *et al.* (2007) Gold nanoparticles capped by peptides. *Materials Science and Engineering: B* 140:187–194.
29. Xie H, *et al.* (2003) Critical flocculation concentrations, binding isotherms, and ligand exchange properties of peptide-modified gold nanoparticles studied by UV-visible, fluorescence, and time-correlated single photon counting spectroscopies. *Anal Chem* 75:5797–5805.
30. El-Sayed IH, Huang X, El-Sayed MA (2005) Surface plasmon resonance scattering and absorption of anti-EGFR antibody conjugated gold nanoparticles in cancer diagnostics: Applications in oral cancer. *Nano Lett* 5:829–834.
31. Liu Y, Franzen S (2008) Factors determining the efficacy of nuclear delivery of antisense oligonucleotides by gold nanoparticles. *Bioconjug Chem* 19:1009–1016.
32. Sandhu KK, McIntosh CM, Simard JM, Smith SW, Rotello VM (2002) Gold nanoparticle-mediated transfection of mammalian cells. *Bioconjug Chem* 13:3–6.
33. Liu Y, *et al.* (2007) Synthesis, stability, and cellular internalization of gold nanoparticles containing mixed peptide-poly(ethylene glycol) monolayers. *Anal Chem* 79:2221–2229.
34. Astriab-Fisher A, Sergueev DS, Fisher M, Shaw BR, Juliano RL (2000) Antisense inhibition of P-glycoprotein expression using peptide-oligonucleotide conjugates. *Biochem Pharmacol* 60:83–90.
35. Pierce TL, White AR, Tregear GW, Sexton PM (2005) Peptide-oligonucleotide hybrids in antisense therapy. *Mini Rev Med Chem* 5:41–55.
36. Muratovska A, Eccles MR (2004) Conjugate for efficient delivery of short interfering RNA (siRNA) into mammalian cells. *FEBS Lett* 558:63–68.
37. Allinquant B, *et al.*(1995) Downregulation of amyloid precursor protein inhibits neurite outgrowth in vitro. *J Cell Biol* 128:919–927.
38. Arar K, Aubertin AM, Roche AC, Monsigny M, Mayer R (1995) Synthesis and antiviral activity of peptide-oligonucleotide conjugates prepared by using N alpha-(bromoacetyl)peptides. *Bioconjug Chem* 6:573–577.
39. Astriab-Fisher A, Sergueev D, Fisher M, Shaw BR, Juliano RL (2002) Conjugates of antisense oligonucleotides with the Tat and antennapedia cell-penetrating peptides: Effects on cellular uptake, binding to target sequences, and biologic actions. *Pharm Res* 19:744–754.
40. Bongartz JP, Aubertin AM, Milhaud PG, Lebleu B (1994) Improved biological activity of antisense oligonucleotides conjugated to a fusogenic peptide. *Nucleic Acids Res* 22:4681–4688.
41. Degols G, Leonetti JP, Benkirane M, Devaux C, Lebleu B (1992) Poly(L-lysine)-conjugated oligonucleotides promote sequence-specific inhibition of acute HIV-1 infection. *Antisense Res Dev* 2:293–301.
42. Lemaitre M, Bayard B, Lebleu B (1987) Specific antiviral activity of a poly(L-lysine)-conjugated oligodeoxyribonucleotide sequence complementary to vesicular stomatitis virus N protein mRNA initiation site. *Proc Natl Acad Sci USA* 84:648–652.
43. Troy CM, Derossi D, Prochiantz A, Greene LA, Shelanski ML (1996) Downregulation of Cu/Zn superoxide dismutase leads to cell death via the nitric oxide-peroxynitrite pathway. *J Neurosci* 16:253–261.
44. Soukchareun S, Tregear GW, Haralambidis J (1995) Preparation and characterization of antisense oligonucleotide-peptide hybrids containing viral fusion peptides. *Bioconjug Chem* 6:43–53.
45. Henke E, *et al.* (2008) Peptide-conjugated antisense oligonucleotides for targeted inhibition of a transcriptional regulator in vivo. *Nat Biotechnol* 26:91–100.
46. Demers LM, *et al.* (2000) A fluorescence-based method for determining the surface coverage and hybridization efficiency of thiol-capped oligonucleotides bound to gold thin films and nanoparticles. *Anal Chem* 72:5535–5541.
47. de La Torre BG, Albericio F, Saison-Behmoaras E, Bachi A, Eritja R (1999) Synthesis and binding properties of oligonucleotides carrying nuclear localization sequences. *Bioconjug Chem* 10:1005–1012.
48. Taton TA, Mirkin CA, Letsinger RL (2000) Scanometric DNA array detection with nanoparticle probes. *Science* 289:1757–1760.
49. Fisher AA, *et al.* (2002) Evaluating the specificity of antisense oligonucleotide conjugates. A DNA array analysis. *J Biol Chem* 277:22980–22984.
50. Benimetskaya L, *et al.* (2002) Protamine-fragment peptides fused to an SV40 nuclear localization signal deliver oligonucleotides that produce antisense effects in prostate and bladder carcinoma cells. *Bioconjugate Chem* 13:177–187.
51. Yang N, Zhang L, Kazanian HH (2005) L1 retrotransposon-mediated stable gene silencing. *Nucl Acids Res* 33:e57.
52. Pante N, Kann M (2002) Nuclear pore complex is able to transport macromolecules with diameters of about 39 nm. *Mol Biol Cell* 13:425–434.
53. Frens G (1973) Controlled nucleation for the regulation of the particle size in monodisperse gold solutions. *Nat Physical Science* 241:20.
54. Hurst SJ, Lytton-Jean AK, Mirkin CA (2006) Maximizing DNA loading on a range of gold nanoparticle sizes. *Anal Chem* 78:8313–8318.